

Liquid-Infused Slippery Stainless Steel Surface Prepared by Alcohol-Assisted Femtosecond Laser Ablation

Yao Fang, Jiale Yong, Yang Cheng, Qing Yang, Xun Hou, and Feng Chen*

Nepenthes-inspired liquid-infused slippery surface (LISS) attracts great attention because it can repel different kinds of liquid and shows great stability. However, the vast majority of LISSs are realized on polymer materials which limit the applications. Here, a kind of universal method to directly construct porous micro/nanostructures on any kind of materials to realize LISS is put forward. As an example, abundant micro/nanohole structures are built on stainless steel surface by alcohol-assisted femtosecond laser ablation. Then, LISS is achieved on stainless steel, which shows slippery property to variety of liquid with different chemical composition. The velocity of water droplet slipping on LISS can be tuned by water droplet volume, LISS tilt angle, and lubricant type. Some potential applications of the LISS are demonstrated by some simple experiments. Flexible movement of magnetic water droplet is realized on the LISS by controlling magnetic field. The LISS shows good antifouling performance to green alga. Moreover, the porous structures are very stable in different harsh environments. This alcohol-assisted femtosecond laser irradiation method successfully constructs porous micro/nanostructures on different kinds of materials. Thus, this work can promote the applications of LISS in droplet manipulation, microfluidics, antifouling surface, and so on.

1. Introduction

Liquid-repellent materials attract great attention because of a wide range of applications, such as self-cleaning coating,[1] water/oil separation, [2] anti-icing surface, [3] microfluidic devices, [4] and so on. [5-8] During the past two decades, superhydrophobic surface is the hottest topic in the field of surface wettability and has been studied extensively.[9-14] It has been demonstrated that the air layer between the water droplet and the superhydrophobic surface is a critical factor for the

Dr. Y. Fang, Dr. J. Yong, Prof. X. Hou, Prof. F. Chen State Key Laboratory for Manufacturing System Engineering and Shaanxi Key Laboratory of Photonics Technology for Information School of Electronic Science and Engineering Xi'an Jiaotong University Xi'an 710049, P. R. China E-mail: chenfeng@mail.xjtu.edu.cn Dr. Y. Cheng, Prof. Q. Yang School of Mechanical Engineering

Xi'an Jiaotong University Xi'an 710049, P. R. China

The ORCID identification number(s) for the author(s) of this article can be found under https://doi.org/10.1002/admi.202001334.

DOI: 10.1002/admi.202001334

superhydrophobic property.[15] The water droplet can only contact the top point of rough structures, which is called Cassie contacting state.[16] However, the air layer is unstable when it suffers from high pressure, high humidness, or even shaking, which can cause the loss of superhydrophobicity. Moreover, superhydrophobic surface can only repel water but fail to repel low surface tension liquid.[17,18]

Because of the slippery property of nepenthes' pitcher, insects cannot stand on the pitcher but slip into the pitcher to be digested. The slippery property benefits from the liquid lubricated layer on the pitcher surface. [19,20] This kind of slippery surface is called liquid-infused slippery surface (LISS). Compared to the air layer of superhydrophobic surface, the liquid layer of LISS is more stable. LISS shows more advantages than superhydrophobic surface, such as anti-various-liquid, pressure stability, and self-healing property.[21-23] Inspired by nepenthes' pitcher, Wong et al. firstly put forward three stand-

ards which must be reached to prepare LISS. [20] First, porous micro/nanostructures are needed to firmly lock the lubricant to form the lubricant layer on the substrate surface. Second, the substrate surface must be more easily wetted by the lubricant rather than the liquid which is planned to be repelled. Third, the repelled liquid must be insoluble in the lubricant. How to construct porous micro/nanostructures is the key to prepare LISS. In recent years, upon these three standards, lots of functional LISSs have been prepared to meet different requirements in practical applications. [24-26] Up to now, the vast majority of LISSs are realized on polymer materials, because it is much easier to construct porous structures on polymer than other materials.^[22,27–31] However, polymer materials are not suitable in some harsh environments including high temperature, high pressure, and some special application fields. Metal materials are widely used in agriculture, construction, medicine, and our daily life. Realizing LISS on metal materials can tremendously widen the application fields of LISS. Some methods are applied to prepare LISS on metal materials, such as hydrothermal method, anodic oxidation, laser ablation, and so on.[32-34] Compared to other methods, laser ablation is an environmentally friendly and universal method. Yong et al. constructed porous structures and realized LISS on polymer materials by femtosecond laser ablation. [32] Jiao at al. prepared LISS on aluminum alloy by femtosecond laser ablation.[35] However, there is no

porous structures on the laser-ablated aluminum alloy. Because of the absence of porous structures, the lubricant cannot be locked stably on the LISS, which has a strong impact on the stability of LISS. Up to now, how to develop an universal method to construct porous structures and realize LISS on different kinds of material, especially on metal materials, is still challenging and desperate in need.

Here, porous micro/nanostructures are produced on stainless steel by one-step alcohol-assisted femtosecond laser irradiation. After further fluoroalkylsilane modification, the surface shows quasi-superhydrophobicity and oleophilicity. After silicone oil infusion, it shows slippery property to different liquid including deionized water, ink, milk, blood, and egg white which have different chemical composition and viscosity. The slipping

velocity increases with the increasing water droplet volume, increasing LISS tilt angle, and decreasing lubricant kinematic viscosity. The porous structures on stainless steel surface can remain the same even after high temperature, high pressure, mechanical friction, and strong organic solvent soaking treatment. Magnetic field controlled movement of microdroplet is realized on the prepared LISS. The LISS shows good antifouling property to green alga. Moreover, this alcohol-assisted femtosecond laser ablation method is universal to construct porous micro/nanostructures on several kinds of materials including metal (stainless steel, nickel), glass, and polymer (shape memory polymer (SMP), polydimethylsiloxane (PDMS)). Thus, this universal method will widen the preparation and applications of LISS, especially on some hard material surface.

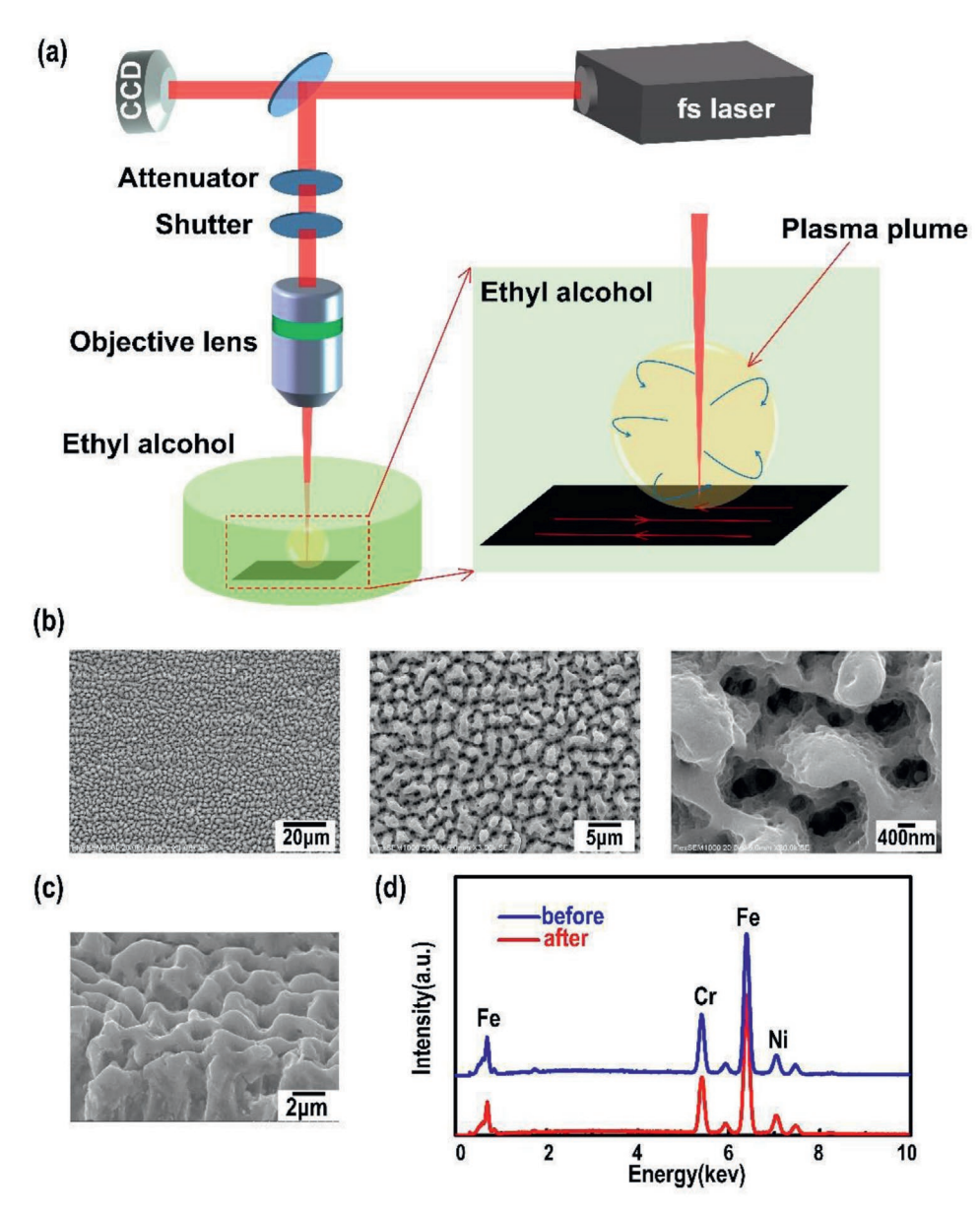


Figure 1. a) Schematic illustration for alcohol-assisted femtosecond laser processing on stainless steel. Surface topography and chemical composition of the femtosecond laser irradiated stainless steel. Typical SEM images: b) top view of different magnifications and c) sectional view. d) EDXS results of the stainless steel before and after femtosecond laser ablation.

2. Results and Discussion

Stainless steel is widely used in agriculture, construction, medicine, and our daily life. Compared to polymer, stainless steel shows more excellent properties, including organic solvents resistance, heat resistance, corrosion resistance, high toughness, and high mechanical strength. Surprisingly, porous microstructures can be directly generated on the stainless steel surface by alcohol-assisted femtosecond laser ablation. The schematic illustration of the alcohol-assisted femtosecond laser ablation process is shown in Figure 1a. As shown in Figure 1b, a mass of papillae with the size ranging from 1 to 4 µm are randomly distributed on the laser-ablated surface. Different from the typical in-air femtosecond laser-induced papillae which have hierarchical rough microstructures (Figure S1, Supporting Information), the top surface of our obtained papillae is relatively smooth. That is because the sputtering particles are rarely deposited on these papillae. The sectional scanning electron microscopy (SEM) image indicates that the height of these papillae reaches up to several micrometers (Figure 1c). Importantly, abundant microholes with the height of several micrometers are constructed around these papillae. These holes range from 0.5 to 2 µm in size. Numerous nanoholes and nano rough structures are observed in these microholes. The structural porosity of the porous stainless steel was about 45.7%, which is estimated from the processed SEM image as shown in Figure S2 (Supporting Information). These micropapillae and micro/nanoholes are of great benefit to store and lock lubricant. The chemical composition of the stainless steel remains unchanged after the alcohol-assisted femtosecond laser ablation, as shown in the energy-dispersive X-ray spectroscopy (EDXS) result (Figure 1d). Thus, these excellent properties of stainless steel which are mentioned above are maintained after alcohol-assisted femtosecond laser ablation.

The ambient environment (ethanol alcohol) of laser ablation is of great importance in the generation of microholes

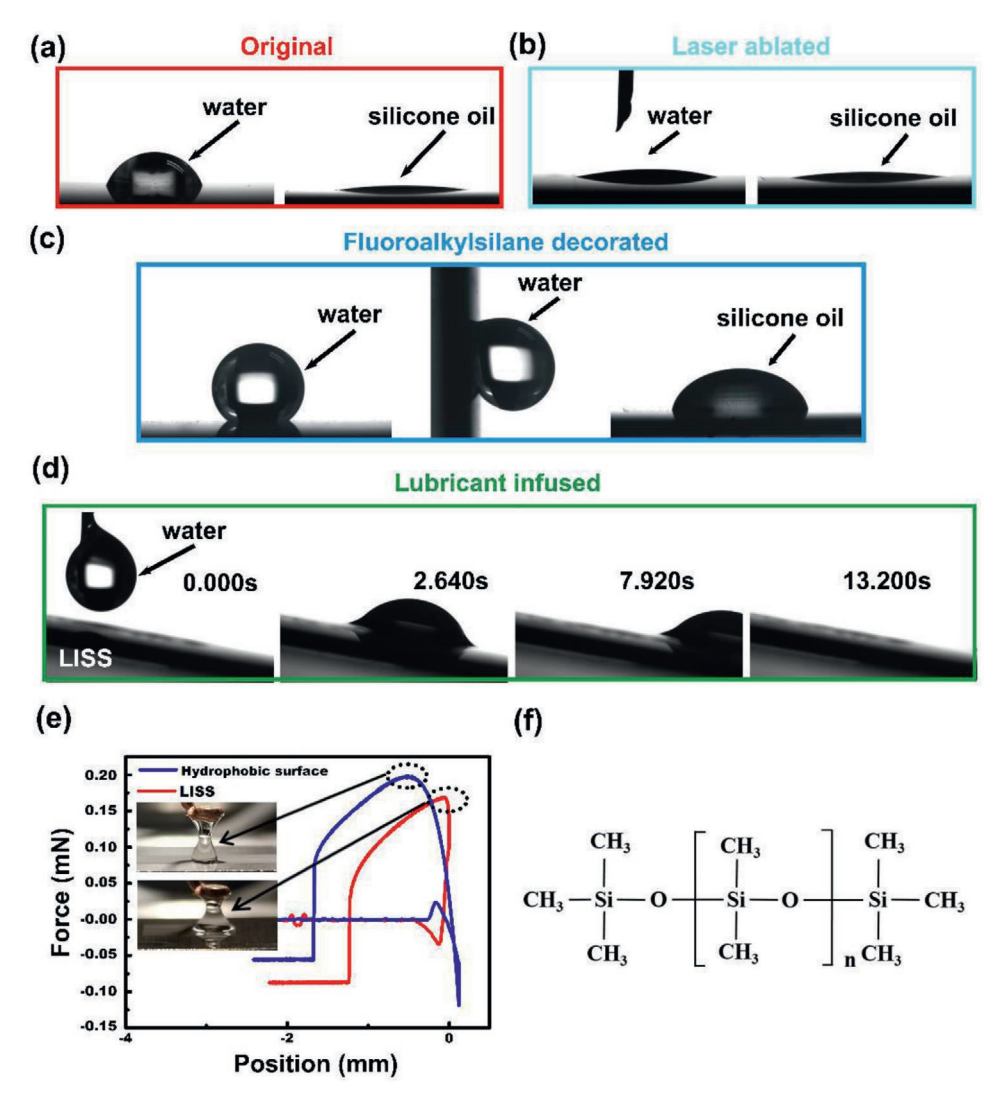


Figure 2. Typical wettability test of stainless steel. a) Original stainless steel. b) After laser irradiation in ethyl alcohol. c) After fluoroalkylsilane modification. d) After silicone oil infusion. e) Typical force—position curves for the hydrophobic surface and LISS. Insets are the critical states of the droplet just leaving the hydrophobic surface and LISS. f) Chemical structure of silicone oil.

structures. Such microholes are not observed on the stainless steel surface that is ablated by femtosecond laser in air (Figure S1, Supporting Information). When femtosecond laser is focused on the interface of stainless steel and ethyl alcohol, the stainless steel is ablated and a plasma plume is generated immediately through nonlinear multiphoton absorption, as shown in Figure 1a insert.[36] Because of the continuous laserinduced vaporizing of the stainless steel and the restriction effect of the ethyl alcohol, a shock wave was produced by the adiabatically expands of the plasma plume at a supersonic velocity in the plasma plume. An additional pressure was created by the shock wave, which caused the immediate increase of the temperature and pressure of the plasma plume.[37-40] Meanwhile, many microbubbles are generated. These special microholes are produced through the synergistic effect of the high-temperature and high-pressure plasma plume and the microbubbles expansion. Moreover, because of the dispersion of ejected particles by ethyl alcohol, these microholes are not covered but retained after the laser ablation process and show a smooth surface.

To obtain a slippery surface which can repel various liquid, the substrate must be more easily wetted by lubricant liquid rather than water. It is the best that the substrate is hydrophobic and oleophilic. The oleophilic property can make it easier to infuse the lubricant into the porous structures, whereas the hydrophobic property can keep the lubricant staying stable in the porous structures and keep it from replacing by other liquid. The original stainless steel shows hydrophilicity and oleophilicity. As shown in **Figure 2**a, the water contact angle (WCA) is $70^{\circ} \pm 1.5^{\circ}$, and silicone oil CA (OCA) is $8.5^{\circ} \pm 0.5^{\circ}$. After laser ablation, the laser-induced

porous structures enhance the wettability of stainless steel (Figure 2b). The WCA is $13^{\circ} \pm 0.5^{\circ}$, which is not beneficial to prepare LISS. The OCA $(9.5^{\circ} \pm 0.5^{\circ})$ has no significant change. Fluoroalkylsilane modification is used to transfer the hydrophilic porous stainless steel to hydrophobic one. After fluoroalkylsilane modification, fluorine was observed on the porous stainless steel (Figure S3, Supporting Information), and the WCA increases to $143^{\circ} \pm 1^{\circ}$ (Figure 2c). The modified porous stainless steel is defined as hydrophobic sample (HS). The silicone oil droplet on HS has a much smaller OCA of 59° ± 0.5°. Therefore, the HS shows inverse wettability (hydrophobicity and oleophilicity) to water and silicone oil. If the stainless steel is not ablated by femtosecond laser, fluoroalkylsilane decorated flat stainless steel only shows a smaller WCA (115.5° \pm 0.5°), as shown in Figure S4 (Supporting Information). Thus, both the laser ablation and the fluoroalkylsilane modification are indispensable. After silicone oil infused in the HS, the LISS is prepared and shows different adhesion to water droplet from HS. In the vertical direction, both HS and LISS show high adhesion. As shown in Figure 2e, the curves show the force that the cantilever is subject to during the whole test process. The water droplet was put on the cantilever in advance. At this situation, the force was set at zero. The water droplet was lowered down, touched the sample surface, and then lifted up. When the water droplet was lifted up, it was deformed and then divided into two droplets because of the high adhesion in vertical direction, as shown in Figure 2e insets. However, in tangential direction, HS and LISS show inverse adhesion to a water droplet. As shown in Figure 2c, even when the HS was set upright, the water droplet cannot

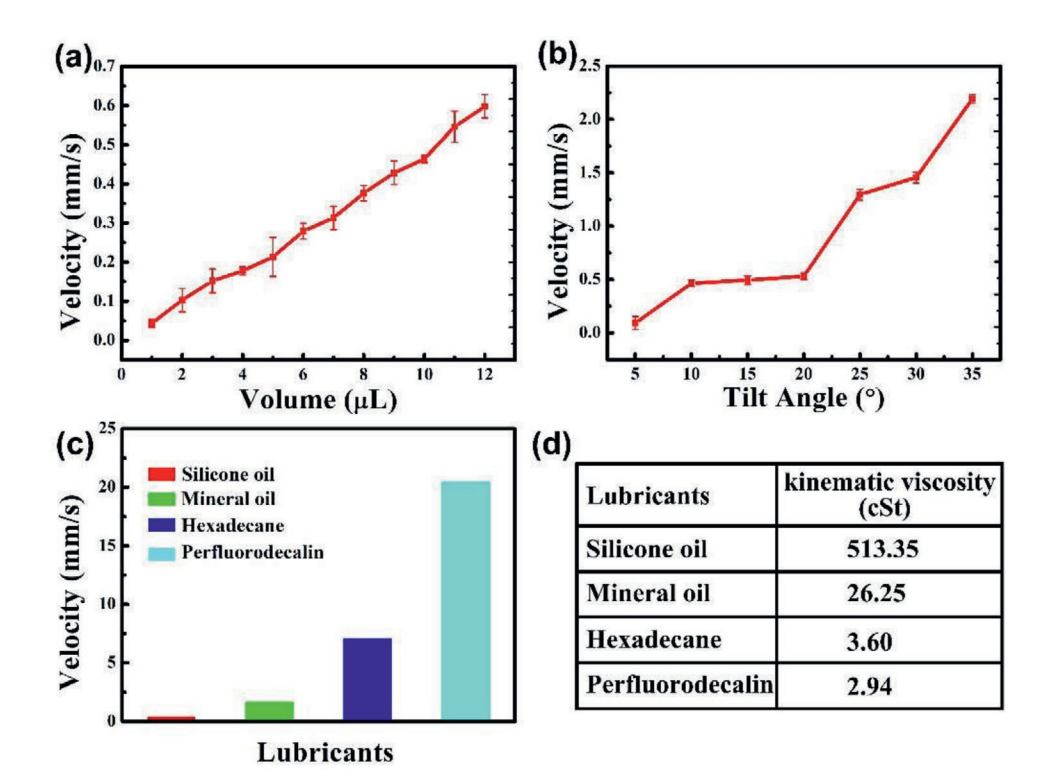


Figure 3. Slippery property of the LISS. a) Velocity as a function of the water droplet volume, and b) the tilt angle of LISS. c) Velocity of water droplet (10 μL) on the different lubricants infused LISS. d) Kinematic viscosity of these different lubricants.

roll down, which indicates a really high adhesion. This is because the water droplet can contact firmly with the micropapillae surface because of the absence of rough structures on these papillae. On the contrary, a water droplet can easily slip down when the LISS was tilted at 10° (Figure 2d). Thus, the LISS shows much smaller adhesion in tangential direction because of the existence of silicone oil layer on LISS.

The velocity of a water droplet slipping on the LISS is important in practical applications. As shown in **Figure 3**a, the velocity increases with the increasing volume of water droplets. There is a positive correlation between the velocity and the tilt angle of LISS (Figure 3b). A bigger volume and a bigger tilt angle mean a bigger tangential component of the water droplet's gravity, which can induce a bigger velocity. The velocity of the water droplet is small because of the big resistance of the LISS, which is caused by the big kinematic viscosity of silicone oil. The kinematic viscosity of lubricants can affect the velocity significantly. As shown in Figure 3c, different lubricants infused LISSs show a huge difference in velocity. The kinematic viscosity of these four lubricants (silicone oil, minerals oil,

hexadecane, perfluorodecalin), which are widely used in reported LISS, [21,41-43] changes from 2.94 to 513.35 cSt, as shown in Figure 3d. Smaller kinematic viscosity induces smaller resistance between the LISS and the water droplet, which results in bigger velocity. The average velocity of water droplets on LISS can be adjusted by the volume of water droplet, the tilt angle of LISS, and the type of lubricant.

The as-prepared LISS can repel various compound liquid (e.g., drinking water, milk, ink, blood, egg white) which are very common in our daily life, as shown in **Figure 4a**. Despite their difference in chemical composition, density, and viscosity, these liquid droplets show similar sliding property on the LISS. When the LISS was tilted at 10°, liquid droplets could slip down freely without any residual. This is beneficial for the infused silicone oil layer which is firmly locked by the hydrophobic porous structure. The slippery lubricant layer can repel different kinds of liquid once the liquid is insoluble in the lubricant.

Because the LISS shows very low adhesion in tangential direction to different liquid, the droplets on the as-prepared LISS can be easily controlled to move. Thus, the LISS can be

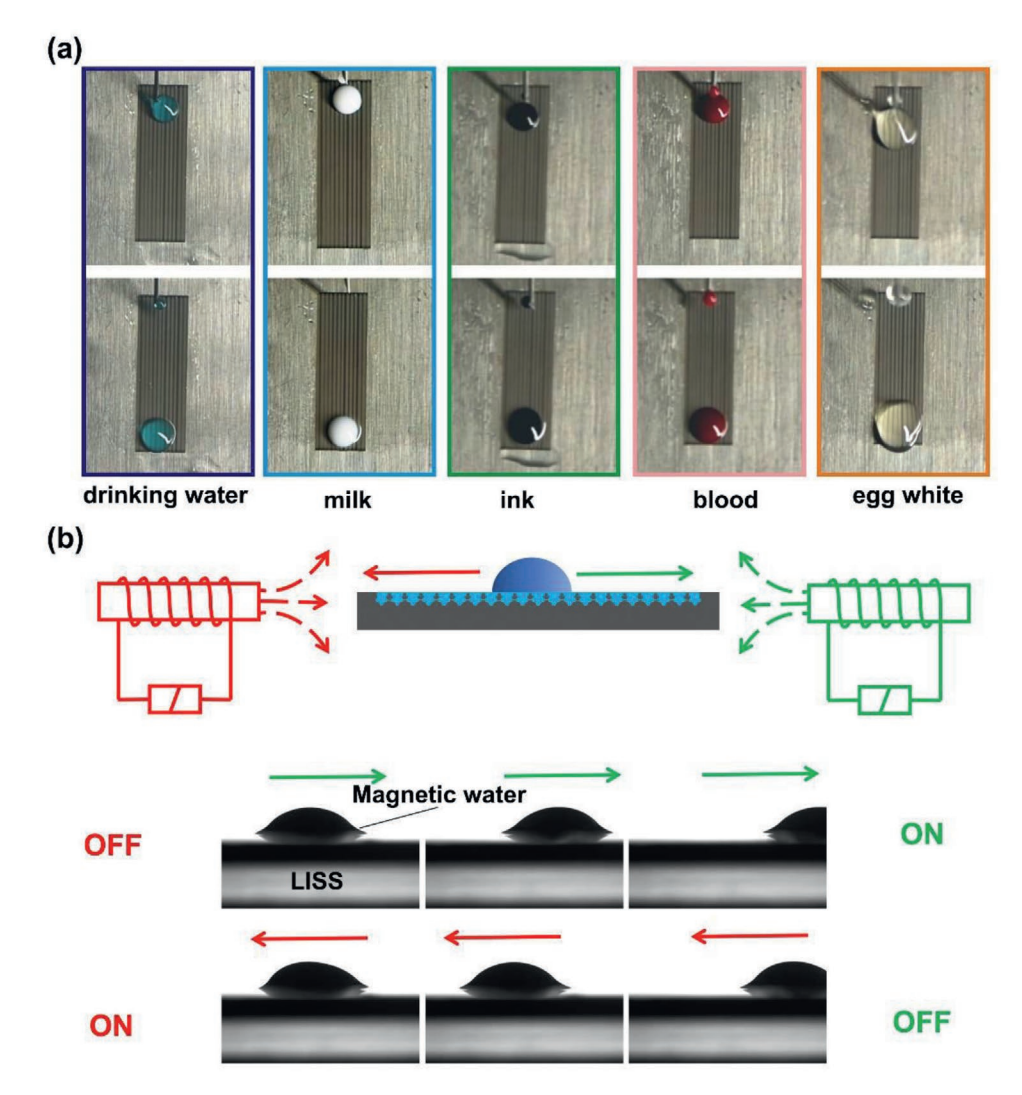


Figure 4. a) Optic images of various liquids before and after sliding down the as-prepared slippery stainless steel surface: drinking water dyed with methylene blue; milk; ink; blood; egg white. b) Controllable movement of a magnetic water droplet by controlling magnetic field.

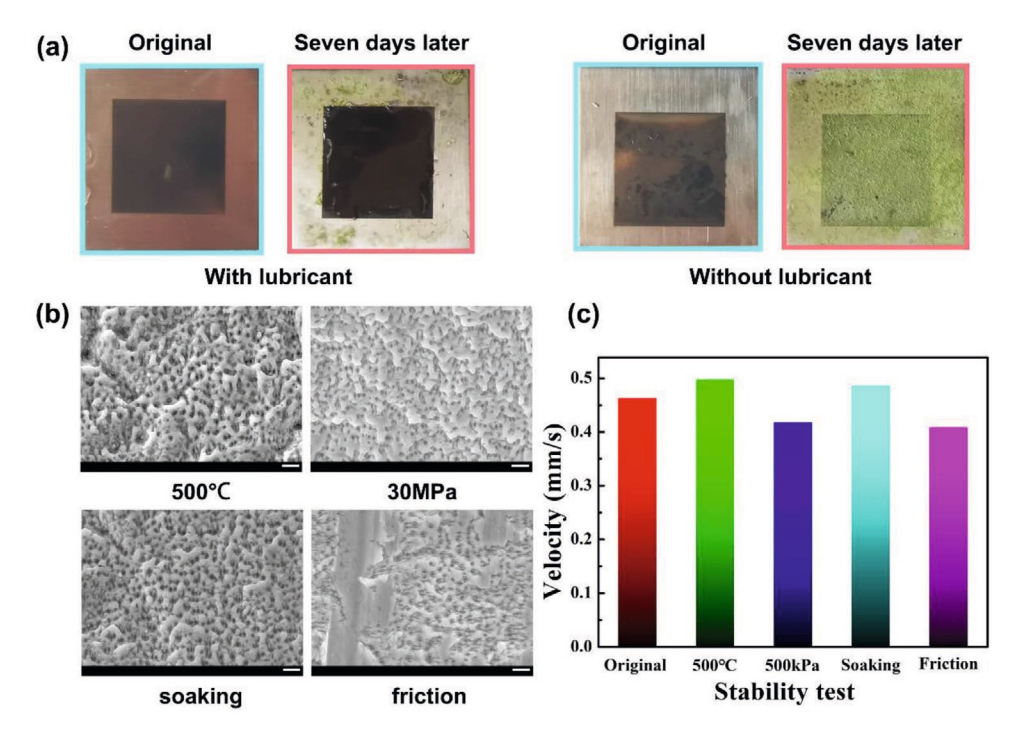


Figure 5. a) Antifouling property of LISS stainless steel to alga. b) SEM images of stainless steel surface after some harsh environments treatment: high temperature of 500 $^{\circ}$ C for 1 h; high pressure of 30 MPa for 1 d; strong organic solvent soaking for 1 d; mechanical friction for 50 times by sand paper. The scale bar is 2 μ m. c) Slippery property after harsh environments treatment.

applied in microdroplet smart manipulation. Magnetic field is a typical noncontacting intelligent controlling method. As an example, magnetic field controlling movement of microdroplet is carried out on the LISS. As shown in Figure 4b, a water droplet that was premixed with magnetic powders was placed on the LISS in advance. The droplet can be controlled to move as expected through manipulating magnetic field. When the magnetic field (21 mT) in the right was turned on, the droplet moved to the right with the velocity of 0.32 mm s⁻¹. Once the droplet reached the destination, the magnetic field should be turned off on both sides. The droplet started to move immediately to the left once the magnetic field in the left was turned on. The movement of the magnetic water droplet is quick response, flexible, and programmable.

Green alga is very common in vast sea area and the inland water. It can attach on ships, bridge pier, and other water flotation devices, which will affect the normal use of these equipment. The as-prepared LISS shows good antifouling performance to green alga, as shown in Figure 5a. Each sample has both untreated flat stainless steel surface and laser-ablated porous surface. One is coating with silicone oil, whereas the other one is used as original. After soaking in the water with green alga for 7 d, the green alga grew on the whole surface of the sample without silicone oil. On the sample with silicone oil, the flat part was partly covered by green alga while the LISS kept cleaning state. The experiment results verify that both the laser-ablated structure and the silicone oil are indispensable for the great antifouling property. The laser-ablated structure can keep the silicone oil exist on the surface for a long time. Because of the existence of silicone oil layer, the LISS shows an excellent property to repel green alga.

Because the LISS was prepared directly based on the porous stainless steel, the stability of LISS is usually judged by the performance of the porous stainless steel. The laser-induced porous structures on stainless steel surface are very robust. They were maintained even after the samples suffered from different harsh environment treatments, as shown in Figure 5b. After storing in high temperature of 500 °C for 1 h, pressing under high pressure of 30 MPa for 1 d, and soaking in 10% (v/v) chloroform ethanol solution for 1 d, respectively, abundant micro/nanoholes still existed on these surfaces. There were a few scratches distributing randomly on the sample surface after 50 abrasion cycles. This cannot be avoided during serious wear. But at other places, many micro/nanoholes were still the same. After infusing silicone oil, each treated surface shows an excellent slippery property, as shown in Figure 5c. There is only a very slight change of the velocity of a water droplet slipping on the treated sample. These results are from the excellent properties of stainless steel material.

The ethyl alcohol-assisted femtosecond laser irradiation can be universally applied to construct porous micro/nanostructures on various types of materials including metal (stainless steel, nickel), glass, and polymer, as shown in Figure 6. The laser ablating parameters are a little different from that of the ablating of stainless steel. The laser power was set at 120 mW for glass, 80 mW for nickel, 70 mW for PDMS, and SMP. For hydrophilic materials (metals and glass), the laser-induced porous microstructures need to be modified by fluoroalkylsilane before obtaining slippery property. In contrast, the step of fluoroalkylsilane modification is needless in the preparation process of LISS for hydrophobic materials (PDMS). Thus, LISS can be realized on various materials to meet different applications.

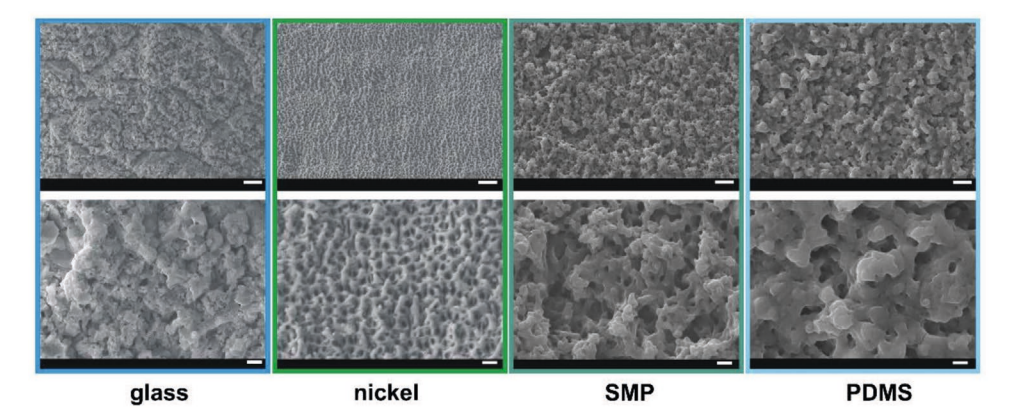


Figure 6. SEM images of different materials fabricated by femtosecond laser in ethyl alcohol. The scale bar is 4 μ m in the first row and 1 μ m in the second row.

3. Conclusion

In conclusion, alcohol-assisted femtosecond laser ablation is proposed as a kind of universal method for preparing LISS on kinds of materials. As an example, porous micro/nanostructure is constructed on stainless steel surface though alcohol-assisted femtosecond laser ablation. After fluoroalkylsilane modification and lubricant infusion, LISS is realized on stainless steel. The as-prepared LISS shows stable slippery property for both water and other compound liquid. The velocity can be adjusted by water droplet volume, LISS tilt angle, and lubricant type. It was proved that the LISS could be applied in microdroplet manipulation, microfluidics, antifouling surface, and so on. A flexible movement of magnetic liquid droplet is achieved on the LISS by controlling magnetic field. The stainless steel LISS shows excellent repellent property to green alga. The porous structures are very stable in different harsh environments. Moreover, this method can be applied in the preparation of LISS on various materials including metal, glass, and polymer. Thus, this work can expand the application fields of LISS to different application environment by selecting different substrate of different chemical and physical properties.

4. Experimental Section

Alcohol-Assisted Femtosecond Laser Processing: A regenerative amplified Ti:sapphire laser system (Coherent Libra-usp-he) was used to construct porous microstructures on a 304 stainless steel (China Baowu Steel Group) surface. The stainless steel sheet with the thickness of 1 mm was previously fixed on the bottom of a glass container which was filled with ethyl alcohol. The glass container was mounted on a precision mobile platform which was controlled by a computer program. The femtosecond laser beam (center wavelength = 800 nm, frequency = 1 kHz, and pulse width = 50 fs) was focused on the stainless steel surface by a microscope objective lens (20×, NA = 0.45, Nikon). The laser power was 80 mW. The diameter of the crater that is formed by one femtosecond laser pulse is about 7 μm, as shown in Figure S5 (Supporting Information). The typical line-by-line laser ablating processing was used. The scanning speed was set at 2000 $\mu m\ s^{-1}.$ The interval of each scanning line was set at 2 µm. After laser ablation, the sample was cleaned in an ultrasonic bath for 10 min by ethyl alcohol and deionized water, respectively.

LISS Preparation: The alcohol-assisted femtosecond laser processing results in the formation of abundant microholes on the surface of stainless steel sheet. The laser-structured stainless steel

sheet was immersed in 2 vol% fluoroalkylsilane (1H,1H,2H,2Hperfluorodecyltrimethoxysilane, Aladdin) solution (in alcohol) for 12 h to lower the surface energy. Then, the sample was stored in an oven at 100 °C for 4 h. Different lubricants, including silicone oil ((CH₃)3SiO(Si(CH₃)₂O)nSi(CH₃)₃, Tianjin Tianli Chemical Reagent Co.), mineral oil (C₁₂H₄Cl₆, Aladdin), hexadecane (C₁₆H₃₄, Tianjin Institute of Chemical Reagents), and perfluorodecalin (C₁₀F₁₈, J&K Scientific GmbH), were used to infuse into the laser-induced microscale pores. Enough lubricant was dripped on the structured stainless steel surface. After the lubricant wetting and infusing into the porous structures, the sample was placed vertically to remove the excess lubricant. As a typical lubricant, silicone oil is selected to prepared LISS to study the property of stainless steel LISS in this article. The chemical structure of silicone oil is shown in Figure 2f. The chemical structures of another lubricants are shown in Figure S6 (Supporting Information).

Stability Test and Characterization: Each abrasion cycle means pulling the sample to move 10 cm on a sand paper (1000 meshes), with a weight of 100 g on the sample (2 cm \times 2 cm), as shown in Figure S7 (Supporting Information). The samples were immersed in the water with green alga for 7 d to test the antifouling property. The average velocity of the water droplet is calculated from the snapshots which are taken by a high-speed camera with 100 frames s⁻¹. SEM images were obtained by using a Flex 1000 SEM (Hitachi, Japan). The wettability of sample was measured by using a JC2000D CA system (Powereach, China). The adhesive force was tested by a DCAT11 surface tension meter (Dataphysics, Germany).

Supporting Information

Supporting Information is available from the Wiley Online Library or from the author.

Acknowledgements

This work was supported by the National Science Foundation of China (Grant Nos. 61875158 and 61805192), the National Key Research and Development Program of China (Grant no.2017YFB1104700, the International Joint Research Laboratory for Micro/Nano Manufacturing and Measurement Technologies, and the Fundamental Research Funds for the Central Universities.

Conflict of Interest

The authors declare no conflict of interest.



www.advancedsciencenews.com



www.advmatinterfaces.de

Keywords

antifouling, femtosecond lasers, liquid-infused slippery surfaces, porous structures, stainless steel

Received: July 28, 2020 Revised: November 16, 2020 Published online: January 6, 2021

- [1] J. Yong, Q. Yang, F. Chen, D. Zhang, H. Bian, Y. Ou, J. Si, G. Du, X. Hou, Appl. Phys. A 2013, 111, 243.
- [2] J. Yong, Y. Fang, F. Chen, J. Huo, Q. Yang, H. Bian, G. Du, X. Hou, Appl. Surf. Sci. 2016, 389, 1148.
- [3] S. Farhadi, M. Farzaneh, S. A. Kulinich, Appl. Surf. Sci. 2011, 257, 6264
- [4] X. Bai, Q. Yang, Y. Fang, J. Zhang, J. Yong, X. Hou, F. Chen, Chem. Eng. J. 2020, 383, 123143.
- [5] J. Jeevahan, M. Chandrasekaran, G. B. Joseph, R. B. Durairaj, G. Mageshwaran, J. Coat. Technol. Res. 2018, 15, 231.
- [6] L. Zhang, H. Kwok, X. Li, H. Z. Yu, ACS Appl. Mater. Interfaces 2017, 9, 39728.
- [7] G. Wen, Z. Guo, W. Liu, Nanoscale 2017, 9, 3338.
- [8] L. Z. Guan, M. C. Gutiérrez, M. J. Roldán-Ruiz, R. Jiménez, M. L. Ferrer, F. del Monte, Adv. Mater. 2019, 31, 1903418.
- [9] J. Yong, C. Zhang, X. Bai, J. Zhang, Q. Yang, X. Hou, F. Chen, Adv. Mater. Interfaces 2020, 7, 1901931;
- [10] Y. Fang, J. Yong, F. Chen, J. Huo, Q. Yang, J. Zhang, X. Hou, Adv. Mater. Interfaces 2018, 5, 1701245.
- [11] M. I. Jamil, X. Zhan, F. Chen, D. Cheng, Q. Zhang, ACS Appl. Mater. Interfaces 2019, 11, 31532.
- [12] C. Zhou, Z. Chen, H. Yang, K. Hou, X. Zeng, Y. Zheng, J. Cheng, ACS Appl. Mater. Interfaces 2017, 9, 9184.
- [13] J. Yong, Q. Yang, F. Chen, D. Zhang, U. Farooq, G. Du, X. Hou, J. Mater. Chem. A 2014, 2, 5499.
- [14] Y. Fang, J. Yong, F. Chen, J. Huo, Q. Yang, H. Bian, G. Du, X. Hou, Appl. Phys. A 2016, 122, 827.
- [15] I. A. Larmour, S. E. J. Bell, G. C. Saunders, Angew. Chem., Int. Ed. Engl. 2007, 119, 1740.
- [16] A. B. D. Cassie, S. Baxter, Trans. Faraday Soc. 1944, 40, 546.
- [17] L. Wen, Y. Tian, L. Jiang, Angew. Chem., Int. Ed. Engl. 2015, 54, 3387.
- [18] Y. Wu, J. Feng, H. Gao, X. Feng, L. Jiang, Adv. Mater. 2019, 31, 1800718.
- [19] H. Chen, P. Zhang, L. Zhang, H. Liu, Y. Jiang, D. Zhang, Z. Han, L. Jiang, *Nature* 2016, 532, 85.

- [20] T. S. Wong, S. H. Kang, S. K. Tang, E. J. Smythe, B. D. Hatton, A. Grinthal, J. Aizenberg, *Nature* 2011, 477, 443.
- [21] J. Li, E. Ueda, D. Paulssen, P. A. Levkin, Adv. Funct. Mater. 2019, 29, 1802317
- [22] J. Yong, F. Chen, Q. Yang, Y. Fang, J. Huo, J. Zhang, X. Hou, Adv. Mater. Interfaces 2017, 4, 1700552.
- [23] C. Huang, Z. Guo, J. BionicEng. 2019, 16, 769.
- [24] J. Kamei, H. Yabu, Adv. Funct. Mater. 2015, 25, 4195.
- [25] U. Manna, D. M. Lynn, Adv. Mater. 2015, 27, 3007.
- [26] S. Amini, S. Kolle, L. Petrone, O. Ahanotu, S. Sunny, C. N. Sutanto, S. Hoon, L. Cohen, J. C. Weaver, J. Aizenberg, N. Vogel, A. Miserez, Science 2017, 357, 668.
- [27] S. Wu, L. Zhou, C. Chen, L. A. Shi, S. Zhu, C. Zhang, D. Meng, Z. Huang, J. Li, Y. Hu, D. Wu, Langmuir 2019, 35, 13915.
- [28] U. Manna, N. Raman, M. A. Welsh, Y. M. Zayas-Gonzalez, H. E. Blackwell, S. P. Palecek, D. M. Lynn, Adv. Funct. Mater. 2016, 26, 3599.
- [29] X. Zhou, Y.-Y. Lee, K. S. L. Chong, C. He, J. Mater. Chem. B 2018, 6, 440
- [30] P. Juuti, J. Haapanen, C. Stenroos, H. Niemelä-Anttonen, J. Harra, H. Koivuluoto, H. Teisala, J. Lahti, M. Tuominen, J. Kuusipalo, P. Vuoristo, J. M. Mäkelä, Appl. Phys. Lett. 2017, 110, 161603.
- [31] T. Guo, P. Che, L. Heng, L. Fan, L. Jiang, Adv. Mater. 2016, 28, 6999.
- [32] J. Yong, J. Huo, Q. Yang, F. Chen, Y. Fang, X. Wu, L. Liu, X. Lu, J. Zhang, X. Hou, Adv. Mater. Interfaces 2018, 5, 1701479.
- [33] M. J. Coady, M. Wood, G. Q. Wallace, K. E. Nielsen, A.-M. Kietzig, F. Lagugné-Labarthet, P. J. Ragogna, ACS Appl. Mater. Interfaces 2018, 10, 2890.
- [34] H. Li, X. Feng, Y. Peng, R. Zeng, Nanoscale 2020, 12, 7700.
- [35] Y. Jiao, X. Lv, Y. Zhang, C. Li, J. Li, H. Wu, Y. Xiao, S. Wu, Y. Hu, D. Wu, J. Chu, Nanoscale 2019, 11, 1370.
- [36] G. Yang, Prog. Mater. Sci. 2007, 52, 648.
- [37] S. Bashir, M. S. Rafique, C. S. Nathala, W. Husinsky, Appl. Surf. Sci. 2014, 290, 53.
- [38] M. V. Shugaev, C.-Y. Shih, E. T. Karim, C. Wu, L. V. Zhigilei, Appl. Surf. Sci. 2017, 417, 54.
- [39] N. Ali, S. Bashir, Umm-i-Kalsoom, N. Begum, M. S. Rafique, W. Husinsky, Appl. Surf. Sci. 2017, 405, 298.
- [40] G. Li, J. Li, C. Zhang, Y. Hu, J. Chu, W. Huang, D. Wu, ACS Appl. Mater. Interfaces 2015, 7, 383.
- [41] P. B. Weisensee, Y. Wang, H. Qian, D. Schultz, W. P. King, N. Miljkovic, Int. J. Heat Mass Transfer 2017, 109, 187.
- [42] S. Sett, X. Yan, G. Barac, L. W. Bolton, N. Miljkovic, ACS Appl. Mater. Interfaces 2017, 9, 36400.
- [43] S. Peppou-Chapman, C. Neto, ACS Appl. Mater. Interfaces 2018, 10,